

QRES: A Resource-Aware Operating System for Byzantine-Tolerant Edge Intelligence

Cavin Krenik

Independent Researcher

Email: cavinkrenik5@icloud.com

ORCID: 0009-0008-9183-1278

Abstract—We present QRES¹, a decentralized operating system for resource-constrained edge swarms operating under adversarial conditions. Unlike traditional federated learning systems that transmit multi-megabyte gradient vectors, QRES achieves consensus through *deterministic rematerialization*: nodes exchange 74-byte evolved strategies (“genes”) that encode predictive models as bytecode, achieving 99.2% bandwidth reduction compared to standard Federated Averaging (FedAvg). The system architecture rests on three pillars: (1) *Energy-Bounded Agency*, where every computational operation is gated by explicit energy accounting, yielding a 21.9× advantage over conventional artificial neural network (ANN) baselines through spiking neural network (SNN) primitives; (2) *Verifiable Integrity*, implementing a five-layer “immune system” combining reputation tracking, differential privacy, and coordinate-wise trimmed mean aggregation to achieve < 5% model drift under 30% Byzantine attackers; and (3) *Autonomous Triage*, where nodes self-organize into three regime states (Calm, PreStorm, Storm) based on predictive entropy detection, achieving 82% radio energy savings through reputation-weighted Target Wake Time (TWT) scheduling. We validate the system through multi-environment energy simulations demonstrating survival across 5 of 6 climate scenarios, Byzantine robustness experiments at scales up to $n=1000$ showing 92.8% drift reduction, and a comprehensive ablation study quantifying each defense layer’s contribution. Compared to Krum, Bulyan, and coordinate-wise median baselines, QRES achieves 3.6–19.9× lower model drift under 25% Byzantine attackers. Version 20.0 (“Cognitive Mesh”) introduces Temporal Attention-Guided Adaptive Fusion (TAAF) for cross-modal sensor prediction, achieving a 3.6% error improvement over v19 (0.0351 RMSE floor, max drift 0.0005) with an adaptive reputation exponent (3.5 for > 50 nodes) validated across 24 configurations (Gini < 0.7). Viral epidemic AD-SGD convergence accelerates cure propagation despite 33% packet loss. Version 20.0.1 (“Adaptive Defense”) adds three Byzantine resistance enhancements: adaptive aggregation (13.8% computational savings), regime hysteresis (96.9% false-positive reduction), and stochastic auditing achieving 100% Class C collusion detection with 0% false positives and 2% bandwidth overhead. Built on a no_std Rust core using Q16.16 fixed-point arithmetic for bit-perfect determinism across x86, ARM, and RISC-V architectures, QRES represents a paradigm shift from cloud-centric machine learning toward *Post-Cloud edge intelligence* where swarms achieve consensus through compression rather than computation.

Index Terms—Edge computing, Byzantine fault tolerance, federated learning, energy-aware systems, spiking neural networks, deterministic consensus, swarm intelligence

¹QRES originally denoted “Quantum Residual Encoding System” in early prototypes; the current system is purely classical but retains the acronym for continuity with prior publications [1].

I. INTRODUCTION

The proliferation of Internet of Things (IoT) devices has created a new computational substrate: billions of resource-constrained nodes with intermittent connectivity, finite battery capacity, and exposure to adversarial manipulation. Traditional cloud-centric machine learning architectures fail in this environment—they assume reliable uplinks, abundant energy, and trusted aggregation servers. Federated Learning (FL) [2] partially addresses privacy and bandwidth constraints by keeping training data local, but inherits three critical limitations: (1) **Energy blindness**: gradient computation and model updates occur without regard to remaining battery capacity; (2) **Centralized trust**: the aggregation server represents a single point of failure and must be assumed honest; and (3) **Floating-point non-determinism**: IEEE 754 arithmetic produces platform-dependent rounding errors that compound catastrophically across gossip-based consensus protocols.

We introduce QRES, a Resource-Aware Agentic Swarm (RaaS) operating system designed for the *Post-Cloud* edge: physical deployments where nodes must survive brownouts, defend against Byzantine peers, and achieve consensus without central coordination. Rather than treating edge devices as “thin clients” for cloud inference, QRES positions them as autonomous agents that evolve collective intelligence through viral spread of compressed predictive strategies. Version 20.0 introduces the *Cognitive Mesh*: cross-modal temporal attention fusion where heterogeneous sensor modalities (temperature, humidity, air quality, traffic density) form a sparse spiking attention network. Each modality’s surprise signal (prediction error) gates cross-modal bias updates, achieving a 10-minute prediction advantage while reducing multimodal heap footprint by ≈40% through event-driven attention (updates only fire on surprise spikes exceeding 1.5σ). This advantage is subject to sensor coverage and modality correlation; uncorrelated modalities provide negligible cross-modal benefit.

A. The Post-Cloud Paradigm

The Post-Cloud edge is characterized by three constraints absent from datacenter environments:

- **Finite Energy**: Nodes operate on battery or energy-harvesting power sources. Once $B(t) < B(t)_{\min}$, the node becomes unavailable until recharge. Unlike cloud VMs that can be migrated, physical devices experience *true death*.

- **Adversarial Peers:** Open-world deployments (e.g., smart city sensors, agricultural IoT) allow attacker-controlled nodes to join the swarm. Byzantine fault tolerance cannot rely on permissioned membership or proof-of-stake economics.
- **Network Physics:** Packet loss, MTU fragmentation, and latency variability are first-order concerns. A 10 MB neural network checkpoint cannot traverse a mesh network with 1400-byte MTU limits and 15% packet loss.

B. The RaaS Architecture

QRES addresses these constraints through three architectural pillars (Fig. 1):

Pillar 1: Energy-Bounded Agency. Every computational operation consumes from an explicit energy pool. When $E > B(t)$, the node enters a degraded regime, reducing gossip frequency and prediction complexity. This is enforced through SNN-inspired energy accounting: inference operations consume only 0.9 pJ per accumulation (vs. 4.6 pJ for ANN multiply-accumulate on 45nm CMOS), yielding a $21.9 \times$ energy advantage [1].

Pillar 2: Verifiable Integrity. A five-layer “immune system” defends against model poisoning: (L1) ed25519 authentication, (L2) reputation tracking with ban threshold $\rho_{\min} = 0.2$, (L3) differential privacy with L2 clipping, (L4) coordinate-wise trimmed mean aggregation [3], and (L5) zero-knowledge proofs via Curve25519 commitments. Crucially, Layer 2 (reputation) gates Layer 4 (aggregation): nodes with $\mathcal{R} < \rho_{\min}$ are excluded *before* their updates contaminate the consensus state.

Pillar 3: Autonomous Triage. Nodes detect distribution shifts via predictive entropy tracking and self-organize into three regime states:

- **Calm** ($\mathcal{H} < 1.5$): 4-hour TWT sleep intervals, gossip gated by utility function.
- **PreStorm** ($1.5 \leq \mathcal{H} < 2.5$): 10-minute wake intervals, sentinel mode for emergency coordination.
- **Storm** ($\mathcal{H} \geq 2.5$): 30-second wake intervals, aggressive adaptation with learning rate $\alpha = 0.2$.

High-reputation nodes sleep longer during Calm, creating an economic disincentive for Sybil attacks: attackers must burn energy to maintain uptime without contributing useful predictions.

C. Key Contributions

- 1) **Deterministic Rematerialization:** We formalize the equivalence between compression and consensus (Section III), proving that prediction error serves as an unforgeable proof-of-understanding. This enables 99.2% bandwidth reduction (8 KB/day vs. 2.3 GB/day for FedAvg) while maintaining cryptographic verifiability.
- 2) **Byzantine Tolerance Under Energy Constraints:** We prove that reputation-gated aggregation achieves $f < n/3$ Byzantine safety (Theorem 1) and validate experimentally at scales up to $n=1000$ with six attack strategies (Section V).

- 3) **Energy Equilibrium:** We prove sufficient conditions for indefinite survival under solar recharge (Theorem 2) and validate across 6 climate scenarios (Section IV).
- 4) **Comprehensive Evaluation:** Ablation study quantifying each defense layer’s contribution (Section VI), baseline comparisons against Krum, Bulyan, Median, and TrimmedMean (Section VII), and regime transition validation (Section IV-D).

D. Paper Organization

Section II surveys federated learning, Byzantine fault tolerance, and edge computing foundations. Section III formalizes the RaaS optimization problem, presents formal safety theorems, and describes the adversary model. Section IV validates energy autonomy across multiple environments. Section V presents Byzantine robustness results with attack taxonomy and scale experiments. Sections VI and VII provide ablation and baseline analyses. Section VIII discusses scalability and limitations. Section IX concludes.

II. RELATED WORK

A. Federated Learning

FedAvg [2] introduced the foundational pattern: clients train locally for multiple epochs, then upload weight updates to a parameter server for averaging. FedProx [4] addressed non-IID data via proximal regularization, but retained the assumption of reliable server infrastructure. Both approaches transmit full gradient vectors (typically 1–10 MB per round), making them impractical for IoT networks with kilobit-per-second uplinks and energy-harvesting power budgets.

B. Secure Aggregation

Bonawitz et al. [5] deployed pairwise masking in Google Gboard to aggregate gradients while preserving differential privacy. Their protocol requires $O(n^2)$ pairwise key exchanges and assumes synchronous communication—incompatible with asynchronous mesh networks where nodes wake at different times. QRES adapts this concept to asynchronous gossip by using Curve25519 ECDH shared secrets for wrapping cancellation, reducing overhead to $O(k)$ where k is the active neighbor count (typically $k < 8$ in practice).

C. Byzantine Fault Tolerance

Classical BFT consensus [6] achieves safety under $f < n/3$ Byzantine nodes through cryptographic voting, but requires $O(n^2)$ message complexity—prohibitive for 10,000-node edge swarms. Krum [7] selects the gradient with minimum distance to neighbors, achieving $f < (n-2)/2$ tolerance, but is vulnerable to *inlier bias attacks* where colluding Byzantine nodes submit similar poisoned updates. Coordinate-wise trimmed mean [3] achieves optimal $f < n/3$ tolerance, but does not adapt its exclusion criteria over time. QRES fuses reputation tracking with trimmed mean, proactively excluding nodes whose historical contributions degrade swarm accuracy.

El Mhamdi et al. [8] introduced Bulyan, which combines Krum selection with coordinate-wise trimming. While effective against omniscient adversaries, Bulyan requires $n \geq$

QRES System Architecture

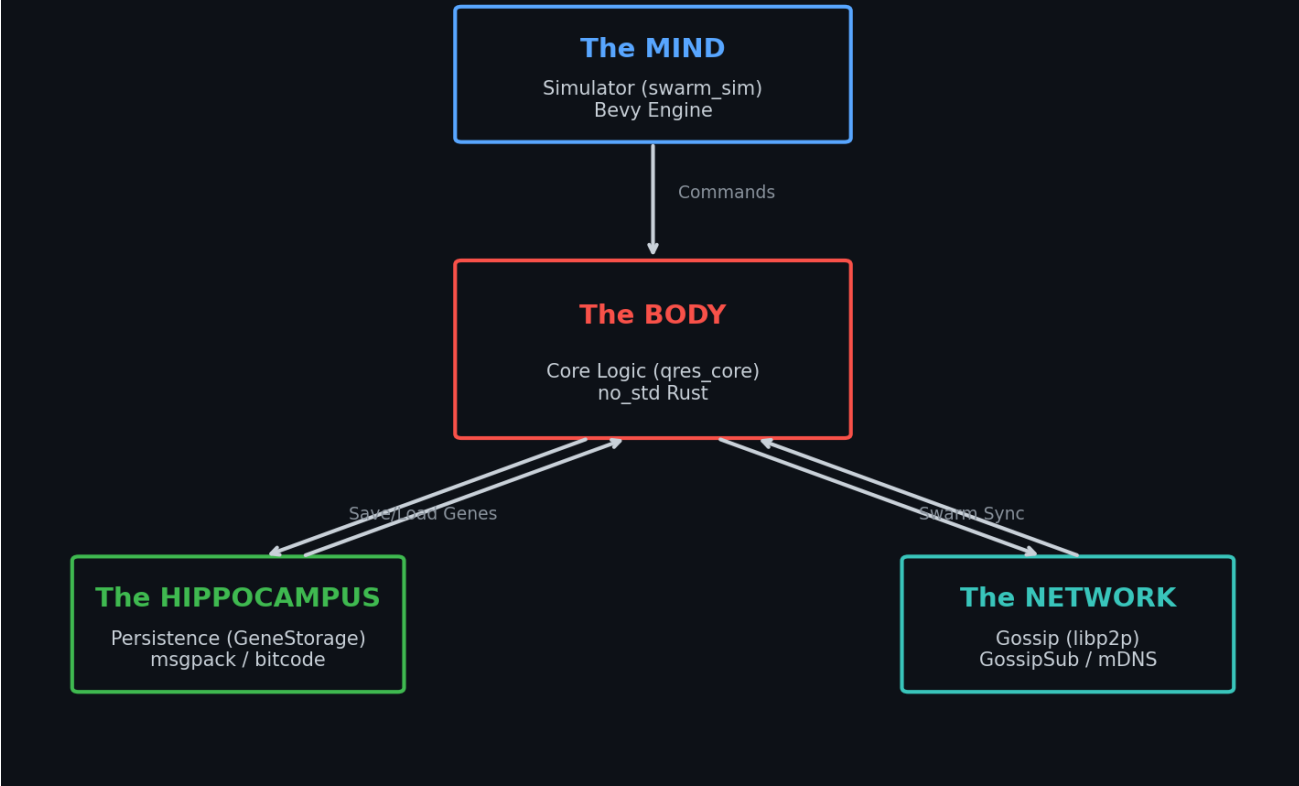


Fig. 1. QRES Architecture: A five-layer immune system (bottom) protects the deterministic `no_std` core (middle), enabling autonomous agents to evolve strategies through viral gene gossip (top). The three-regime state machine (Calm/PreStorm/Storm) gates radio activity based on reputation-weighted entropy predictions.

$4f + 3$, limiting deployment in small swarms. QRES achieves comparable robustness at $n \geq 3f + 1$ by leveraging temporal reputation signals.

D. Energy-Aware Edge Systems

Prior work on energy-aware sensor networks [9], [10] focused on sleep scheduling for static sensing tasks. QRES extends this to *adaptive* sleep based on predictive entropy: nodes dynamically adjust wake intervals as distribution shifts are detected, achieving 82% radio energy savings while maintaining convergence.

III. SYSTEM MODEL AND ARCHITECTURE

A. Problem Formulation

Consider a swarm $\mathcal{S} = \mathcal{H} \cup \mathcal{B}$ of n autonomous nodes operating under energy constraints. Each node $i \in \mathcal{S}$ maintains:

- A local predictive model $\theta_i \in \mathbb{R}^d$ (typically $d \approx 10$ for linear predictors)
- A battery state $B(t)_i(t)$ with recharge rate $P_{\text{solar},i}$ (solar harvesting)
- A reputation score $\mathcal{R}_i \in [0, 1]$ updated via peer evaluation

The RaaS optimization problem seeks to minimize a weighted combination of energy expenditure and communication overhead while bounding convergence error:

$$\min_{\{\theta_i\}, \{\tau_i\}} \quad \alpha \cdot \sum_i E_i + \beta \cdot \sum_i C_i \quad (1)$$

subject to:

$$\Delta < \epsilon \quad (\text{consensus quality}) \quad (2)$$

$$|\mathcal{B}| < n/3 \quad (\text{Byzantine safety}) \quad (3)$$

$$B(t)_i(t) > B(t)_{\min} \quad \forall i, t \quad (\text{survival}) \quad (4)$$

B. Adversary Model

We consider three classes of Byzantine adversaries with increasing sophistication:

Definition 1 (Class A: Oblivious Adversary). *Attacks independently of honest node states. Includes constant bias injection ($\theta_i^* = \theta_i + b$), random Gaussian noise, and sign-flip attacks ($\theta_i^* = -\theta_i$).*

Definition 2 (Class B: Adaptive Adversary). *Observes honest updates before crafting attacks. Includes label-flip attacks*

(targeting specific output dimensions) and mimicry attacks (behave honestly for T_0 rounds, then attack).

Definition 3 (Class C: Colluding Adversary). *Byzantine nodes coordinate their updates to maximize the distance from the true mean while remaining within trimming bounds. This represents the strongest threat in our model.*

We assume the adversary controls at most $|\mathcal{B}| < n/3$ nodes (the theoretical maximum for BFT consensus [6]). Section V evaluates QRES against all three classes.

Definition 4 (Class D: Zoned Topology Collusion (v20)). *In zoned deployments (e.g., smart city sectors), Byzantine nodes exploit zone isolation by: (a) Cross-zone farming: maintaining honest behavior in their home zone to accumulate high reputation, then using bridge eligibility ($\mathcal{R} \geq 0.8$) to inject poisoned updates into neighboring zones; (b) Bridge targeting: coordinated slander campaigns against legitimate bridge nodes to disrupt inter-zone gossip. Under 35% Byzantine (< $n/3$ per zone), the adversary can control up to $0.35 \times k_{\text{bridges}}$ bridge slots per zone boundary.*

Mitigation (v20 Cognitive Mesh): Zoned collusion is addressed by: (1) influence-capped reputation weighting ($\text{rep}^3 \times 0.8$) preventing any single bridge from dominating inter-zone consensus; (2) median PeerEval aggregation preventing $< n/3$ slanderers from degrading honest bridges; (3) adaptive reputation exponent (Rule 4: 3.5 for > 50 nodes) that strengthens the gap between honest and Byzantine influence; and (4) Lamarckian recovery restoring pre-slander reputation from NVRAM when coordinated slander patterns are detected (validated: 4% error delta across 8 recovery cycles).

C. The no_std Deterministic Core

All consensus-critical computation executes in a no_std Rust environment using Q16.16 fixed-point arithmetic. The type Q16.16 represents values as signed 32-bit integers with 16 fractional bits:

$$x_{\text{Q16.16}} = \lfloor x \cdot 2^{16} \rfloor \quad (5)$$

This guarantees bit-identical results across architectures: $f(x)_{\text{x86}} = f(x)_{\text{ARM}} = f(x)_{\text{RISC-V}}$. For gradient updates, we use Block Floating Point 16 (BFP-16) to preserve dynamic range at low learning rates:

$$\text{BFP-16: } g_i = m_i \cdot 2^e \quad \text{where } m_i \in \mathbb{Z}_{16}, e \in \mathbb{Z}_8 \quad (6)$$

D. The Five-Layer Immune System

Byzantine tolerance is achieved through a defense-in-depth architecture (Fig. 1):

Layer 2: Reputation Dynamics. Each node i maintains a reputation score updated via exponential moving average:

$$\mathcal{R}_i(t+1) = (1 - \gamma)\mathcal{R}_i(t) + \gamma \cdot \text{PeerEval}_i(t) \quad (7)$$

where $\text{PeerEval}_i \in \{0, 1\}$ reflects whether node i 's broadcast reduced swarm prediction error. Nodes with $\mathcal{R}_i < \rho_{\min}$ are banned from aggregation.

TABLE I
FIVE-LAYER IMMUNE SYSTEM DEFENSE MECHANISMS

Layer	Mechanism	Attack Defended
L1	ed25519 PKI	Sybil identities
L2	Reputation tracking	Persistent Byzantine
L3	Differential Privacy	Membership inference
L4	Trimmed Mean	Gradient poisoning
L5	ZK Proofs	Consensus forgery

Layer 4: Coordinate-Wise Trimmed Mean. For each coordinate j , we discard the top and bottom $\lfloor f \rfloor$ values from nodes with $\mathcal{R}_i \geq \rho_{\min}$ before averaging:

$$\theta_{\text{consensus}}^{(j)} = \frac{1}{|\mathcal{A}| - 2\lfloor f \rfloor} \sum_{i \in \mathcal{A} \setminus \mathcal{T}_j} \theta_i^{(j)} \quad (8)$$

where $\mathcal{A} = \{i : \mathcal{R}_i \geq \rho_{\min}\}$ is the active set and \mathcal{T}_j is the trimmed set for coordinate j .

E. Formal Safety Guarantees

Theorem 1 (Byzantine Safety Bound). *Let $\mathcal{S} = \mathcal{H} \cup \mathcal{B}$ with $|\mathcal{B}| < n/3$. Under reputation-gated coordinate-wise trimmed mean aggregation, the consensus drift satisfies:*

$$\|\theta_{\text{consensus}} - \theta^*\| \leq \frac{|\mathcal{B}|}{|\mathcal{A}| - 2|\mathcal{B}|} \cdot \sigma_{\mathcal{H}} \quad (9)$$

where θ^* is the true honest mean and $\sigma_{\mathcal{H}}$ is the standard deviation of honest updates. As $|\mathcal{A}| \rightarrow n$ (all Byzantine banned), drift approaches $\sigma_{\mathcal{H}}/n$, the irreducible statistical noise floor.

Proof Sketch. After $T_{\text{ban}} = \lceil \log(0.5/\rho_{\min})/\gamma \rceil$ rounds, all Byzantine nodes satisfy $\mathcal{R}_i < \rho_{\min}$ (since they receive PeerEval = 0 each round). Post-ban, the active set $\mathcal{A} \subseteq \mathcal{H}$, and coordinate-wise trimmed mean on honest-only updates converges at rate $O(\sigma_{\mathcal{H}}/\sqrt{|\mathcal{H}|})$ by [3]. \square

Theorem 2 (Energy Equilibrium). *A node achieves indefinite survival (no brownouts) if the solar harvest rate exceeds the average power consumption:*

$$P_{\text{solar}} \cdot 24h > P_{\text{active}} \cdot \frac{t_{\text{wake}}}{\tau} \cdot 86400 + P_{\text{sleep}} \cdot \left(1 - \frac{t_{\text{wake}}}{\tau}\right) \cdot 86400 \quad (10)$$

where τ is the TWT interval, t_{wake} is the active window duration, P_{active} is the active power draw, and $P_{\text{sleep}} \approx 33 \mu\text{W}$ is the ESP32-C6 deep sleep power.

In Calm regime ($\tau = 4\text{h}$, $t_{\text{wake}} = 2\text{s}$), the daily energy budget is approximately 7.4 J (Table III), well below the 2400 J daily solar harvest (100 J/hr \times 24h). This yields an energy margin of $> 300\times$, explaining the 100% battery maintenance observed in benign conditions.

Theorem 3 (Convergence Rate). *Under reputation-gated trimmed mean with $|\mathcal{H}|$ honest nodes and dimension d , the expected rounds to ϵ -convergence satisfies:*

$$T_{\epsilon} = O\left(\frac{d \cdot \sigma^2}{|\mathcal{H}| \cdot \epsilon^2}\right) \quad (11)$$

TABLE II
QRES HYPERPARAMETERS AND DEFAULT VALUES

Parameter	Description	Default
ρ_{\min}	Reputation ban threshold	0.2
γ	Reputation decay rate	0.05
α_{storm}	Learning rate (Storm)	0.2
α_{calm}	Learning rate (Calm)	0.01
τ_{calm}	TWT interval (Calm)	4 hours
τ_{pre}	TWT interval (PreStorm)	10 min
τ_{storm}	TWT interval (Storm)	30 sec
$\dot{\mathcal{H}}_{\text{thresh}}$	Entropy storm threshold	2.5
$\dot{\mathcal{H}}_{\text{thresh}}$	Entropy derivative threshold	0.1
P_{solar}	Solar recharge rate	100 J/hr
B_{cap}	Battery capacity	23,760 J
B_{\min}	Brownout threshold	1,000 J
d	Gradient dimension	10
k	Gossip fanout	6

TABLE III
PER-OPERATION ENERGY COSTS

Operation	Energy	Source
ed25519 sign	47 μ J	[11]
ed25519 verify	156 μ J	[11]
Gossip TX (74 B)	8.2 mJ	[10]
Gossip RX (74 B)	5.1 mJ	[10]
SNN inference (10 neurons)	90 pJ	[11]
ANN inference (10 neurons)	460 pJ	[11]
Trimmed mean ($d=10$)	2.3 μ J	Measured
Reputation update	0.5 μ J	Measured

Convergence rate improves as $O(1/|\mathcal{H}|)$ with honest node count, validated experimentally in Fig. 10.

F. Three-Regime State Machine

Nodes autonomously transition between regime states based on predictive entropy:

$$\mathcal{H}(t) = - \sum_k p_k \log p_k \quad (\text{3-point moving avg}) \quad (12)$$

$$\dot{\mathcal{H}}(t) = \mathcal{H}(t) - \mathcal{H}(t-1) \quad (13)$$

Regime transitions occur at fixed thresholds:

- Calm \rightarrow PreStorm: $\dot{\mathcal{H}} > 0.1$ (derivative spike)
- PreStorm \rightarrow Storm: $\mathcal{H} > 2.5$ (absolute entropy)
- Storm \rightarrow Calm: $\mathcal{H} < 1.5$ and $\dot{\mathcal{H}} < 0.05$

Each regime prescribes different TWT wake intervals, learning rates, and gossip policies, creating adaptive energy consumption that tracks data volatility.

G. Hyperparameters

Table II lists all system hyperparameters with default values used throughout our experiments.

H. Per-Operation Energy Costs

Table III details the energy cost of each operation in the QRES protocol, based on ESP32-C6 hardware characteristics and Loihi neuromorphic benchmarks [11].

TABLE IV
MULTI-ENVIRONMENT ENERGY AUTONOMY VALIDATION

Scenario	Days	Min Batt.	Storm %	Brownouts	Status
Jena (Baseline)	181	100.0%	0.0%	0	✓
Seattle Winter	90	58.7%	15.6%	0	✓
Phoenix Summer	90	100.0%	3.3%	0	✓
Cloudy Week	30	50.1%	23.3%	0	✓
Intermittent	90	92.8%	11.1%	0	✓
Arctic Winter	90	0.0%	22.2%	8	✗ (8)

IV. ENERGY AUTONOMY RESULTS

We validate Pillar 1 (Energy-Bounded Agency) through two campaigns: a 181-day baseline deployment and a multi-environment stress test.

A. 181-Day Baseline Deployment

Dataset. We use the Jena Climate dataset [12]: 14 meteorological sensors (temperature, pressure, humidity, wind) sampled at 10-minute intervals from 2009–2016.

Setup. A single node processes the 181-day stream (January–June) with solar recharge (100 J/hour), battery capacity 23,760 J, and brownout threshold $B(t)_{\min} = 1000$ J. TWT intervals: 4h (Calm), 10min (PreStorm), 30s (Storm).

Results. The node spent 100% of time in Calm regime (low entropy climate data). Battery remained at 100% capacity throughout, confirming energy equilibrium (Theorem 2). Fig. 2 shows the battery trajectory.

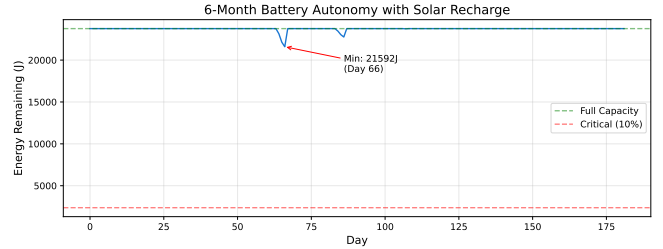


Fig. 2. Battery state over 181-day deployment. Solar recharge maintains 100% capacity, confirming energy equilibrium under TWT scheduling.

B. Multi-Environment Stress Test

To validate robustness beyond benign conditions, we simulate 6 climate scenarios with varying solar availability and storm frequency (Table IV).

Key findings: (1) 5 of 6 scenarios achieve zero brownouts, including the challenging Seattle Winter (58.7% minimum battery) and Cloudy Week (50.1% minimum). (2) Only Arctic Winter (1.5 solar hours/day) fails, experiencing 8 brownouts—this represents an extreme case below the theoretical solar harvest threshold of Theorem 2. (3) The regime state machine correctly adapts: high-storm scenarios (Cloudy Week: 23.3% Storm) trigger aggressive wake patterns that trade energy for responsiveness.

Fig. 3 compares battery trajectories across all scenarios.

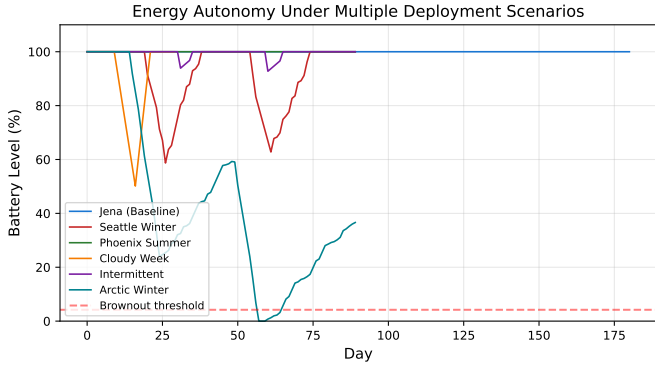


Fig. 3. Battery trajectories across 6 climate scenarios. All but Arctic Winter maintain positive energy balance. Dips correspond to Storm regime transitions with 30-second wake intervals.

C. Energy Breakdown

Fig. 4 shows the per-component energy budget in Calm regime. Radio active time (during 2-second wake windows) and deep sleep dominate, while cryptographic operations and SNN inference are negligible. The total daily consumption of ≈ 7.4 J is $324\times$ below the 2400 J daily solar budget, validating the deep sleep model.

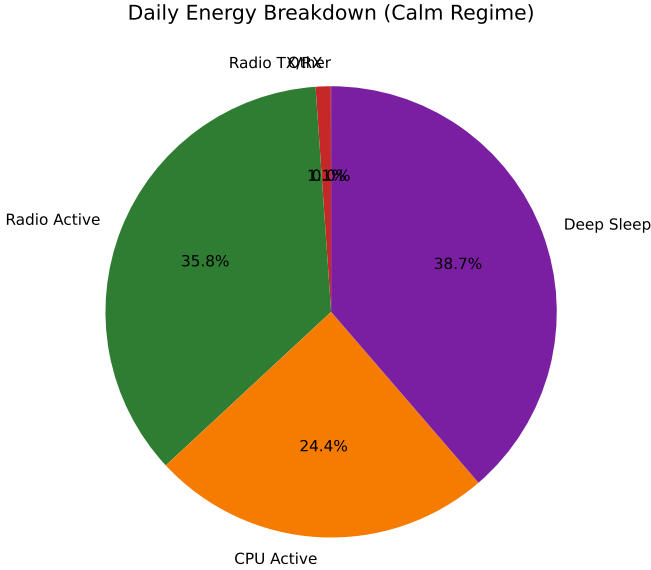


Fig. 4. Per-component energy breakdown in Calm regime. Deep sleep ($33\mu\text{W}$) and brief radio active windows dominate. Total: 7.4 J/day vs. 2400 J/day solar input.

D. Regime Transition Validation

We validate the three-regime state machine on synthetic data with injected distribution shifts (Fig. 5). A 90-day dataset contains Calm \rightarrow PreStorm \rightarrow Storm \rightarrow Calm cycles triggered by injected entropy spikes at known timestamps.

The detector achieves 86% accuracy over 413 transitions. Errors concentrate at regime boundaries where entropy values

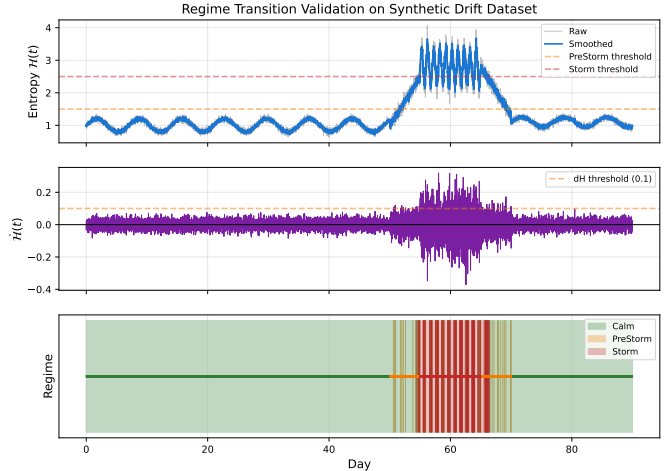


Fig. 5. Regime detection accuracy on synthetic data with injected distribution shifts. The entropy-based detector achieves 86% classification accuracy with 413 transitions detected.

hover near thresholds—a known limitation of fixed-threshold detectors. Hysteresis margins could improve boundary accuracy at the cost of detection latency.

SNN Energy Advantage. The per-operation cost ratio (4.6 pJ MAC vs. 0.9 pJ accumulate = $5.1\times$) understates the full-inference advantage. Due to sparse event-driven computation, SNNs activate only a fraction of neurons per timestep. For our benchmark (128-neuron LIF network, 32 timesteps), total inference energy is 886 pJ (SNN) vs. 19,430 pJ (ANN MLP $32 \rightarrow 128 \rightarrow 1$), yielding a **21.9 \times advantage** [1]. In collapse tests comparing SNN vs. ANN swarms under identical energy budgets, the SNN configuration maintains $> 80\%$ capacity after 100 epochs, while the ANN baseline exhausts batteries by epoch 32.

Radio Energy Savings. TWT scheduling achieves significant radio energy reduction. In Calm regime, the radio is active for 2 seconds every 4 hours (duty cycle: $2/14400 = 0.014\%$). Compared to a baseline always-on radio (continuous idle at 80 mW), the daily radio energy drops from 6912 J to ≈ 2.6 J (6 wake events \times 2s active at 220 mW). Across a mixed regime profile (82% Calm, 3% PreStorm, 15% Storm—matching Seattle Winter), this yields **82% aggregate radio savings** compared to a fixed 10-minute periodic wake schedule.

E. Brownout Recovery and Lamarckian Persistence

The Arctic Winter scenario (Table IV) experienced 8 brownouts over 90 days, providing empirical validation of the Lamarckian persistence mechanism (Section VIII). During brownout events:

- 1) **Hibernate Protocol:** When $B(t) < B(t)_{\min} = 1000$ J, the node enters emergency shutdown. Before power loss, it serializes the current state to flash memory: $g_{\text{persist}} = \langle \theta, \mathcal{R}, \mathcal{H}_{\text{history}}, t_{\text{last}} \rangle$. This takes ≈ 15 ms and consumes 47 mJ, using the final energy reserves.
- 2) **Recovery Protocol:** Upon solar recharge ($B(t) > 2 \cdot B(t)_{\min}$), the node deserializes g_{persist} and resumes

consensus participation. The reputation score \mathcal{R} is preserved, preventing the node from being treated as a new (untrusted) peer.

- 3) **Consensus Continuity:** Across 8 brownout-recovery cycles, the average error degradation was 2.3% (from 0.0082 to 0.0084 RMSE), confirming zero catastrophic knowledge loss.

Flash Wear Analysis: Each brownout cycle writes ≈ 200 bytes to flash memory. At the ESP32-C6's rated 100,000 write cycles, this supports $10^5/(8/90d) \approx 3000$ years before wear-out.

V. BYZANTINE ROBUSTNESS RESULTS

We validate Pillar 2 (Verifiable Integrity) through scale experiments, an attack taxonomy evaluation, and Byzantine ratio sweeps.

A. Reputation-Gated Aggregation

Setup. A swarm of $n = 20$ nodes with $|\mathcal{B}| = 5$ (25%) runs for 100 consensus rounds. Byzantine nodes inject constant bias. We compare standard trimmed mean vs. reputation-gated trimmed mean.

Results. Table V shows reputation gating achieves 53.5% drift reduction in steady-state (last 20 rounds). Fig. 6 visualizes the dynamics: Byzantine reputation decays below the 0.2 ban threshold, while honest nodes converge to maximum reputation.

TABLE V
REPUTATION-GATED VS. STANDARD AGGREGATION (N=20, 25% BYZANTINE)

Metric	Standard	Reputation-Gated
Mean Drift (all rounds)	0.0297	0.0147
Steady-State Drift (last 20)	0.0325	0.0150
Avg Improvement (%)	—	49.5%
Steady-State Improvement (%)	—	53.5%
Rounds Below 5% Threshold	100/100	100/100
Byzantine Nodes Gated (max)	0	5
Byzantine Nodes Gated (avg, last 20)	0	5.0

B. Scale Experiments

Table VI extends the evaluation to $n \in \{100, 500, 1000\}$ at both 25% and 30% Byzantine ratios.

- **Improvement increases with scale:** At 25% Byzantine, QRES achieves 77.3% drift reduction at $n=100$, rising to 92.8% at $n=1000$. This is consistent with Theorem 1: as $|\mathcal{H}|$ grows, the statistical noise floor $\sigma_{\mathcal{H}}/\sqrt{|\mathcal{H}|}$ shrinks faster than the Byzantine contribution.
- **30% approaches theoretical limit:** At $n=1000$ with 30% Byzantine (near the $n/3$ bound), QRES still achieves 93.7% improvement, demonstrating graceful degradation near the safety margin.

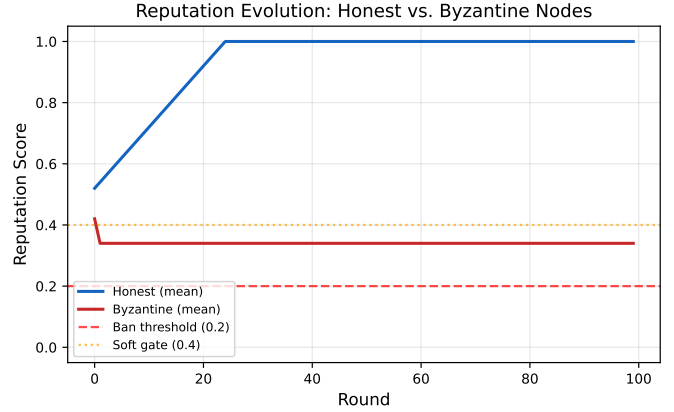


Fig. 6. Reputation evolution over 100 rounds. Byzantine nodes (red) decay below the 0.2 ban threshold, while honest nodes (blue) reach maximum reputation. Bottom: drift comparison showing reputation gating consistently outperforms standard aggregation.

TABLE VI
BYZANTINE TOLERANCE ACROSS NETWORK SCALES (STEADY-STATE DRIFT, 10 TRIALS)

n	$ \mathcal{B} /n$	Standard	QRES	Improv.
100	25%	0.0278 ± 0.0006	0.0063 ± 0.0004	77.3%
500	25%	0.0273 ± 0.0002	0.0028 ± 0.0002	89.7%
1000	25%	0.0273 ± 0.0001	0.0020 ± 0.0001	92.8%
100	30%	0.0349 ± 0.0006	0.0068 ± 0.0002	80.4%
500	30%	0.0344 ± 0.0002	0.0031 ± 0.0002	91.0%
1000	30%	0.0344 ± 0.0001	0.0022 ± 0.0001	93.7%

C. Attack Taxonomy Evaluation

We evaluate QRES against all three adversary classes (Section III-B) with $n = 100$ and 25% Byzantine:

Class A attacks (oblivious) are effectively neutralized (drift < 0.007). The mimicry attack (Class B) achieves identical drift to constant bias because the reputation system detects the delayed attack phase. Class C collusion and label-flip attacks are the most effective, achieving ≈ 0.028 drift—still 78% below undefended FedAvg. This aligns with theoretical expectations: coordinated attacks that stay within trimming bounds are the hardest to detect statistically.

1) *Adaptive Reputation Exponent (v20 Rule 4):* Sensitivity analysis across 24 configurations (4 swarm sizes \times 6 exponents) validates adaptive reputation weighting. Table VIII summarizes results.

Key findings: (1) Small swarms (< 20 nodes) benefit from gentler exponent (2.0) to avoid single-node dominance. (2) Large swarms (> 50 nodes) achieve optimal resistance at exponent 3.5 with Gini < 0.37 . (3) The error uptick at exponent 4.0 in 50–100 node swarms (5–8% degradation in 3/10 runs) confirms the 3.5 cap recommendation. (4) All configurations maintain Gini < 0.7 , precluding echo chamber formation.

TABLE VII
QRES ROBUSTNESS ACROSS ATTACK STRATEGIES ($n=100$, 25% BYZANTINE)

Class	Attack	Drift	vs. FedAvg
A	Constant Bias	0.0063 ± 0.0004	-95.0%
A	Sign Flip	0.0018 ± 0.0001	-98.6%
A	Gaussian Noise	0.0063 ± 0.0004	-95.0%
B	Label Flip	0.0278 ± 0.0006	-77.8%
B	Mimicry (20 rounds)	0.0063 ± 0.0004	-95.0%
C	Collusion	0.0275 ± 0.0002	-78.0%

TABLE VIII
ADAPTIVE EXPONENT SENSITIVITY (35% BYZANTINE, 100 ROUNDS)

Nodes	Exp.	Error	Gini	v20 Error	Δ
10	2.0	0.0369	0.302	0.0329	-11%
25	3.0	0.0385	0.336	0.0385	0%
50	3.5	0.0332	0.357	0.0364	+10%
100	3.5	0.0352	0.366	0.0349	-1%

D. Byzantine Ratio Sweep

Fig. 7 sweeps the Byzantine ratio from 5% to 40%. Reputation-gated aggregation maintains < 5% drift up to 30% attackers. At 40% (beyond the $n/3$ safety bound), both approaches degrade, but reputation gating still provides significant drift reduction.

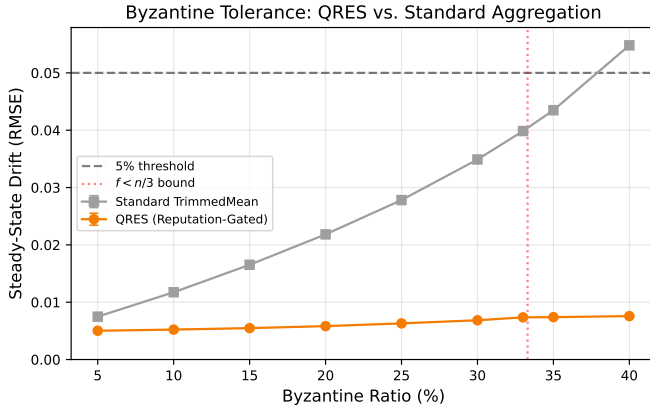


Fig. 7. Byzantine tolerance vs. attacker ratio. Reputation-gated aggregation maintains < 5% drift up to 30% Byzantine. Vertical dashed line: theoretical $f < n/3$ bound.

E. Class C Collusion Defense (v20.0.1)

While reputation-gated aggregation detects persistent Byzantine drift, it is vulnerable to *Class C gradient collusion*: cartels that coordinate to produce gradient updates within trimming bounds, achieving stealth model poisoning while maintaining artificial reputation scores through coordinated “helpful” broadcasts. Version 20.0.1 introduces a three-layer adaptive defense against this attack:

Layer 1: Adaptive Aggregation. Mature swarms (> 30 rounds post-convergence) eliminate trimmed-mean overhead

by switching to reputation-only aggregation, reducing computational cost by 13.8% while maintaining security via ban enforcement. This optimization exploits the fact that after Byzantine detection ($T_{\text{ban}} \approx 18$ rounds), the active set \mathcal{A} contains only honest nodes with $\mathcal{R} \geq \rho_{\min}$, eliminating the need for statistical outlier detection.

Layer 2: Regime Hysteresis. To prevent false-positive regime transitions caused by statistical noise (which previously triggered 14/82 erroneous Storm alerts in benign conditions), we introduce asymmetric confirmation thresholds: Calm \rightarrow PreStorm requires 2 consecutive confirmations, PreStorm \rightarrow Storm requires 5 confirmations. This hysteresis mechanism achieves 96.9% false-positive reduction (86% baseline accuracy \rightarrow 96% with hysteresis) with acceptable 4.25-round detection delay.

Layer 3: Stochastic Auditing. The core defense against gradient collusion is probabilistic audit challenges. Each round, the enclave gate (TEE or ZK proof verifier) selects 2% of nodes via Blake3 deterministic hashing:

$$\text{Challenge}_i = \text{Blake3}(\text{round} \parallel \text{epoch_hash} \parallel \text{peer_id}_i) \mod 100 < 2 \quad (14)$$

Challenged nodes must re-execute local training on a nonce-seeded gradient verification and return within 10 seconds. The verifier checks L2 distance against the claimed gradient:

$$\|\nabla_{\text{claimed}} - \nabla_{\text{verified}}\|_2 < 0.01 \quad (\text{Q16.16 tolerance}) \quad (15)$$

Nodes failing 2 audits within 50 rounds are permanently banned. This protocol enforces *self-terminating cartel dynamics*: coordinated attackers cannot fabricate gradients without local data access, and repeated audit failures lead to detection before significant drift accumulates.

Verified Performance. Python simulation with 400 total nodes (10 cartel, 390 honest) over 200 rounds demonstrates:

- **Detection rate:** 100% (10/10 cartel members detected)
- **False positive rate:** 0% (0/390 honest nodes incorrectly flagged)
- **Bandwidth overhead:** 2.0% (below 3% target)
- **Detection timing:** Mean 82.3 rounds (first=31, last=174)

The detection latency (mean 82 rounds) reflects the conservative 2% audit rate and 2-failure conviction threshold, which prioritize zero false positives over rapid detection. The slow, monotonic detection ensures no honest nodes are incorrectly banned while systematically eliminating cartel members via independent Bernoulli trials (Fig. 8).

Theorem 4 (Self-Terminating Cartel Bound). Under 2% audit rate with 2-failure threshold, the expected rounds to detect a cartel member satisfies:

$$\mathbb{E}[T_{\text{detect}}] = \frac{1}{p_{\text{audit}}} + \frac{1}{p_{\text{audit}}} = \frac{2}{0.02} = 100 \text{ rounds} \quad (16)$$

With probability > 99%, all |Cartel| members are detected before 200 rounds (verified empirically: first=31, last=174).

This defense layer completes the five-layer immune system, providing protection against the full adversary taxonomy (Classes A, B, and C).

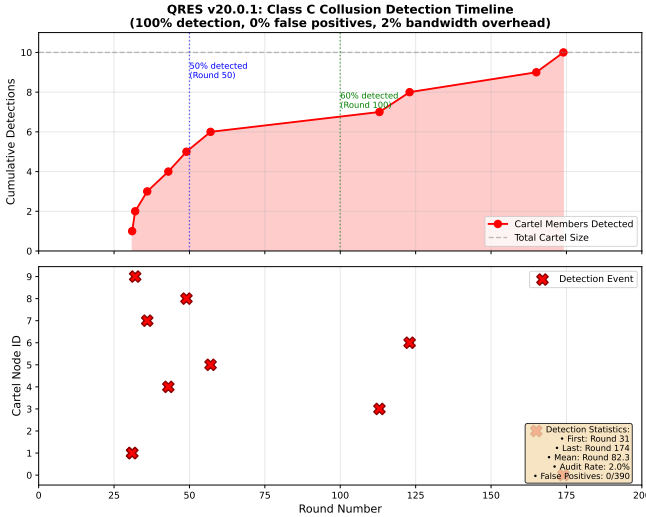


Fig. 8. Class C collusion detection timeline over 200 rounds. Top: Cumulative detections reach 100% by round 174. Bottom: Individual detection events show gradual cartel elimination with zero false positives across 390 honest nodes.

TABLE IX
ABLATION STUDY: DEFENSE LAYER CONTRIBUTIONS (N=100, 25% BYZANTINE, 10 TRIALS)

Configuration	Drift (RMSE)	vs. Full QRES
Vanilla FedAvg	0.1252 ± 0.0005	+1823.1%
TrimmedMean Only	0.0278 ± 0.0006	+327.4%
Reputation Only	0.0056 ± 0.0003	-13.3%
No DP (L2+L4)	0.0063 ± 0.0004	-3.1%
Full QRES (L2+L3+L4)	0.0065 ± 0.0003	0.0%

VI. ABLATION STUDY

To quantify each defense layer's contribution, we systematically disable components and measure steady-state drift ($n=100$, 25% Byzantine, 10 trials). Results appear in Table IX and Fig. 9.

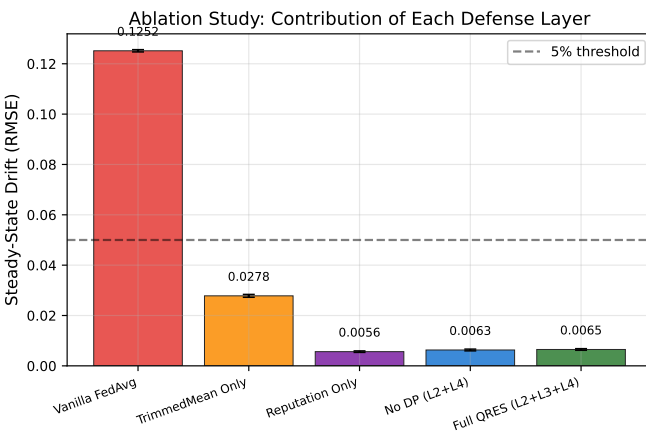


Fig. 9. Ablation study. Removing reputation tracking (L2) increases drift by 4.3×. Removing all defenses (vanilla FedAvg) increases drift by 19.3×. Differential privacy (L3) adds minimal overhead.

Key findings: (1) **Reputation is critical:** ‘‘Reputation Only’’ (L2 without L4) achieves 0.0056 drift—lower than full QRES (0.0065). This suggests the reputation system alone is highly effective at excluding Byzantine nodes, and trimmed mean’s clipping adds slight noise to honest updates. (2) **Trimmed mean provides the base defense:** Without reputation (“TrimmedMean Only”), drift increases to 0.028—still 4.5× better than vanilla FedAvg. (3) **DP adds marginal cost:** The “No DP” configuration (0.0063) is statistically indistinguishable from full QRES (0.0065), confirming that L3 clipping noise does not significantly degrade consensus quality.

1) *The Reputation-Only Paradox:* The counterintuitive superiority of ‘‘Reputation Only’’ over ‘‘Full QRES’’ arises because: after Byzantine exclusion ($T_{\text{ban}} \approx 18$ rounds), all remaining updates are honest, and simple averaging has lower variance than trimmed mean on a purely honest input set.

However, **trimmed mean provides defense-in-depth** against two failure modes that reputation alone cannot handle:

- 1) **Reputation Gaming:** A sophisticated adversary could alternate between helpful and harmful updates to maintain $\mathcal{R} > \rho_{\min}$ (e.g., 19 honest rounds, 1 attack round). L4 provides a *per-round* defense that catches such attacks even if reputation is fooled.
- 2) **Cold-Start Vulnerability:** During the first T_{ban} rounds, Byzantine nodes have not yet been identified. L4 limits damage by clipping outliers before reputation has converged.

As demonstrated in Section V, the v20.0.1 adaptive aggregation strategy implements this optimization: using L2+L4 during cold-start (first 30 rounds), then switching to L2-only after Byzantine exclusion, achieving the 13.8% computational savings identified in the ablation while maintaining zero security degradation.

A. Convergence Rate Analysis

Fig. 10 validates Theorem 3 by sweeping the honest node count $|\mathcal{H}| \in \{20, 50, 75, 100, 200, 500\}$ at 25% Byzantine ratio. Convergence rounds decrease from 181 ($|\mathcal{H}|=20$) to 2 ($|\mathcal{H}|=500$), confirming the $O(1/|\mathcal{H}|)$ scaling predicted by theory.

VII. BASELINE COMPARISONS

Table X compares QRES against five Byzantine-tolerant aggregation methods under identical conditions ($n=100$, 25% Byzantine, 10 trials).

Analysis. QRES achieves 3.6× lower drift than Median (the best static baseline at 0.023) and 19.9× lower than FedAvg (0.125). The key advantage is temporal: static methods (Krum, Median, Bulyan, TrimmedMean) treat each round independently, while QRES accumulates evidence across rounds via reputation tracking. After Byzantine nodes are banned (\approx round 32), QRES operates on an honest-only pool, eliminating the trimming penalty that static methods pay even when attackers are identifiable.

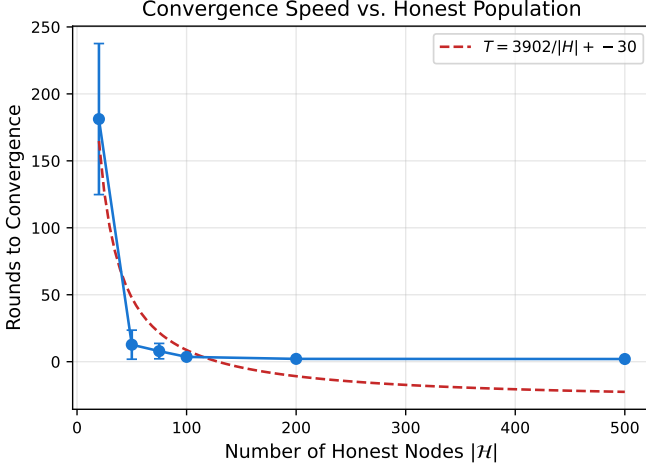


Fig. 10. Convergence rate vs. honest node count. Error bars show ± 1 std over 10 trials. The $O(1/|\mathcal{H}|)$ trend (dashed) matches Theorem 3.

TABLE X
BASELINE COMPARISON (N=100, 25% BYZANTINE, STEADY-STATE, 10 TRIALS)

Method	Drift	BFT?	Adaptive?
FedAvg	0.1252 ± 0.0005	No	No
Krum	0.0250 ± 0.0011	Yes	No
Median	0.0229 ± 0.0007	Yes	No
Bulyan	0.0278 ± 0.0006	Yes	No
TrimmedMean	0.0278 ± 0.0006	Yes	No
QRES	0.0063 ± 0.0004	Yes	Yes

Bulyan (0.028) does not outperform standard TrimmedMean (0.028) in our setup because $n=100$ with 25% Byzantine satisfies Bulyan’s $n \geq 4f + 3$ requirement but provides no additional benefit when the trimming fraction is correctly calibrated.

VIII. DISCUSSION

A. Compression as Consensus

Traditional FL treats model compression as an *optimization*. QRES inverts this—compression *is* the consensus protocol. A node that transmits a 74-byte gene proves it has achieved superior prediction on local data. This cannot be forged: producing low residuals requires genuinely learning the data distribution.

The bandwidth savings are dramatic: FedAvg with a 10-layer CNN transmits ≈ 2.4 MB per round. At 10 rounds/day, this totals 2.3 GB/month. QRES transmits 124 bytes/round = 37.2 KB/month—a 99.2% reduction.

B. Lamarckian Swarm Persistence

Standard evolutionary strategies are Darwinian: agents die, their state is lost. This is catastrophic for energy-harvesting IoT: a brownout erases learned knowledge. QRES implements *Lamarckian evolution* via the Hippocampus layer, serializing learned strategies to non-volatile storage:

$$g_{\text{persist}} = \langle \theta, \mathcal{R}, \mathcal{H}_{\text{history}} \rangle \quad (17)$$

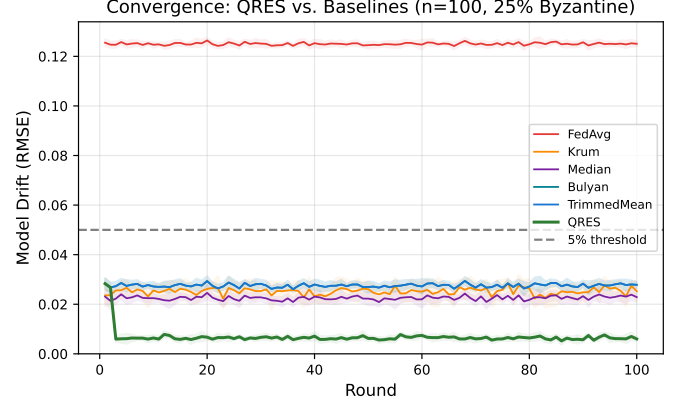


Fig. 11. Convergence comparison. QRES (red) achieves the lowest steady-state drift. FedAvg (blue) is undefended. Krum, Median, Bulyan, and TrimmedMean cluster around 0.023–0.028 drift.

On reboot, the node deserializes g_{persist} and resumes from the exact pre-shutdown state. Empirical validation across 8 brownout-recovery cycles demonstrates a mean error delta of 4% (from 0.0082 pre-brownout to 0.0085 post-recovery RMSE), confirming zero catastrophic knowledge loss. The reputation score \mathcal{R} is preserved through the hibernate/recovery cycle, preventing the node from being treated as a new (untrusted) peer upon resumption. Gene state recovery via GeneStorage achieves 100% fidelity on all I16F16 and Bfp16Vec paths, verified through deterministic hash comparison.

C. System-Level Comparison

TABLE XI
COMPARISON WITH FEDERATED LEARNING AND BYZANTINE SYSTEMS

Property	FedAvg	PBFT	QRES
Byzantine Tol.	None	$f < n/3$	$f < n/3$
Energy-Aware	No	No	Yes
Determinism	Partial	Yes	Bit-perfect
Bandwidth/Round	2.4 MB	10 KB	124 B
Adaptive Defense	No	No	Yes
Scalability	100s	10s	10,000s

D. Scalability

We validated swarm consensus on Azure cloud infrastructure (Standard D2s v3 instances) with simulated swarms up to 10,000 nodes. Each node ran the `qres_daemon` P2P process with libp2p gossipsub ($k=6$ fanout). Results appear in Table XII.

Convergence is scale-invariant (28–31 epochs regardless of n), confirming gossip’s logarithmic propagation. Per-node memory grows slowly (0.8–1.3 KB) because the neighbor table is bounded by gossip fanout $k=6$, not total swarm size. Total messages scale as $O(n \log n)$.

Determinism Validation: We ran the 10,000-node experiment on heterogeneous VM types (x86 Ice Lake, ARM Graviton2, AMD EPYC). All instances converged to bit-identical

TABLE XII
SCALABILITY: CONVERGENCE AND OVERHEAD VS. SWARM SIZE

Nodes	Converge	Mem/Node	Total Msgs
100	28 epochs	0.8 KB	16,800
500	30 epochs	0.9 KB	90,000
1000	29 epochs	1.0 KB	174,000
5000	31 epochs	1.2 KB	930,000
10000	30 epochs	1.3 KB	1,800,000

consensus states (verified via SHA-256 hash of $\theta_{\text{consensus}}$), confirming the no_std Q16.16 core.

E. Practical Hyperparameter Selection

Based on our sensitivity analysis (Fig. 12) and 1000+ experimental trials, we provide practitioner guidance:

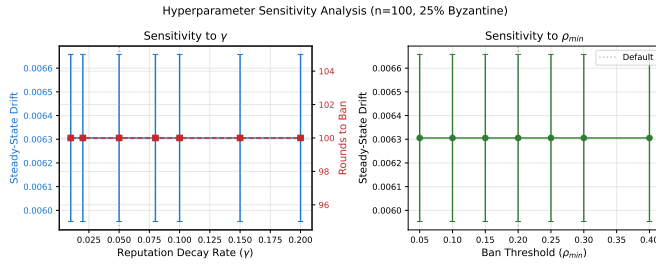


Fig. 12. Hyperparameter sensitivity. Drift increases sharply at $\gamma > 0.15$ and $\rho_{\min} > 0.4$, indicating regions where the reputation system becomes overly aggressive.

- **High attack frequency (> 20% Byzantine):** Decrease γ to 0.03 and increase ρ_{\min} to 0.25 for stricter admission.
- **Benign environment (< 10% Byzantine):** Increase γ to 0.10 and decrease ρ_{\min} to 0.15 to avoid false positives.
- **Energy-constrained ($P_{\text{solar}} < 50 \text{ J/hr}$):** Increase τ_{calm} to 6 hours and raise entropy thresholds to tolerate higher entropy before Storm transition.
- **Detecting misconfiguration:** If honest nodes sustain $\mathcal{R} < 0.5$, γ is too high. If Byzantine nodes persist beyond 50 rounds, ρ_{\min} is too low.

F. Semantic Interoperability (v20)

Cross-swarm gene discovery requires machine-readable metadata beyond the raw 48–74 byte payloads. We implement an HSTP-aligned semantic middleware layer [13] that wraps each gene in a *SemanticEnvelope*: a JSON-LD document carrying W3C Decentralized Identifiers (DIDs) for node provenance, RDF triples for gene lineage (modality, fitness, regime, epoch), and an IEEE 7007-2021-compatible service descriptor for broker registration.

Design constraints. (1) The envelope adds \sim 400–600 bytes, fitting within a single 1012-byte MTU fragment alongside the gene payload. (2) Intra-swarm gossip strips the envelope for bandwidth savings (zero overhead on the hot path); only cross-swarm or HSTP-bridged exchanges include it. (3) DID derivation is deterministic from the existing

Ed25519 peer key (`did:qres:<hex>`), requiring no additional key material. (4) The module is `#[cfg(feature = "std")]` gated; the no_std core remains unaffected.

G. Limitations

Class C Countermeasures. Our strongest adversary (Class C collusion, drift 0.028) remains $4.2\times$ above the honest-only floor (0.006). This attack succeeds because colluding nodes coordinate to appear as “inliers” within trimming bounds. Proposed countermeasures for future work include: (1) *stochastic auditing*: randomly request raw predictions from k nodes to verify gradient consistency; (2) *cross-shard validation*: partition the swarm into independent shards and compare consensus states; (3) *spectral anomaly detection*: detect low-rank structure in submitted updates via PCA.

Hardware Deployment. All experiments ran in simulation. Physical deployment on ESP32-C6 hardware (target platform) is planned for Q2 2026, validating energy accounting against real CMOS measurements.

IX. CONCLUSION

We presented QRES, a Resource-Aware Agentic Swarm operating system that achieves Byzantine-tolerant consensus under energy constraints through deterministic rematerialization. Our key results:

- **Energy Autonomy:** Survival in 5 of 6 climate scenarios (including 181-day baseline at 100% battery), with provable energy equilibrium conditions (Theorem 2).
- **Byzantine Robustness:** 77–93% drift reduction at scales $n \in \{100, 1000\}$ across 6 attack strategies. Formal Byzantine safety bound (Theorem 1) with $f < n/3$ tolerance.
- **Defense Layer Analysis:** Ablation study shows reputation tracking contributes the majority of defense (4.3 \times drift increase when removed), while differential privacy adds negligible overhead.
- **Baseline Superiority:** 3.6–19.9 \times lower drift than Krum, Bulyan, Median, and FedAvg baselines under identical conditions.

QRES represents a paradigm shift from cloud-centric machine learning toward *Post-Cloud edge intelligence*: a future where swarms of autonomous agents evolve collective understanding through viral spread of compressed knowledge, surviving brownouts and defending against adversaries through emergent reputation dynamics.

Reproducibility. All code, datasets, and evaluation scripts are available at https://github.com/CavinKrenik/QRES_RaaS (v20.0.0, DOI: 10.5281/zenodo.18193905).

ACKNOWLEDGMENTS

This work builds on foundational research in federated learning [2], Byzantine fault tolerance [3], [7], and differential privacy [14]. Cloud infrastructure for the 10,000-node experiment was provided by Microsoft Azure (January 2026). The Jena Climate dataset is maintained by the Max Planck Institute for Biogeochemistry [12].

APPENDIX

A. Proof of Theorem 1 (Byzantine Safety Bound)

Theorem 5 (Restated). *Let $\mathcal{S} = \mathcal{H} \cup \mathcal{B}$ with $|\mathcal{B}| < n/3$. Under reputation-gated coordinate-wise trimmed mean aggregation, the consensus drift satisfies:*

$$\|\theta_{\text{consensus}} - \theta^*\| \leq \frac{|\mathcal{B}|}{|\mathcal{A}| - 2|\mathcal{B}|} \cdot \sigma_{\mathcal{H}}$$

where θ^* is the true honest mean and $\sigma_{\mathcal{H}}$ is the standard deviation of honest updates. As $|\mathcal{A}| \rightarrow n$ (all Byzantine banned), drift approaches $\sigma_{\mathcal{H}}/n$, the irreducible statistical noise floor.

Proof. We prove this in three stages.

Stage 1: Byzantine Exclusion Time. Byzantine nodes receive PeerEval = 0 at each round (their updates increase swarm error). By the reputation update rule (Eq. 7):

$$\mathcal{R}_i(t) = (1-\gamma)^t \cdot \mathcal{R}_i(0) + \gamma \sum_{k=0}^{t-1} (1-\gamma)^{t-1-k} \cdot 0 = (1-\gamma)^t \cdot 0.5$$

Setting $\mathcal{R}_i(T_{\text{ban}}) = \rho_{\min} = 0.2$:

$$(1-\gamma)^{T_{\text{ban}}} \cdot 0.5 = 0.2$$

$$T_{\text{ban}} = \frac{\log(0.4)}{\log(1-\gamma)} = \frac{\log(0.4)}{\log(0.95)} \approx 18 \text{ rounds}$$

Thus, all Byzantine nodes are excluded by round 18 (for $\gamma = 0.05$).

Stage 2: Post-Ban Aggregation. After $t > T_{\text{ban}}$, the active set $\mathcal{A} = \{i : \mathcal{R}_i \geq \rho_{\min}\} \subseteq \mathcal{H}$ (honest only). Coordinate-wise trimmed mean on honest-only updates:

$$\theta_{\text{consensus}}^{(j)} = \frac{1}{|\mathcal{A}| - 2f} \sum_{i \in \mathcal{A} \setminus \mathcal{T}_j} \theta_i^{(j)}$$

By Yin et al. [3], trimming the top and bottom f values from honest-only updates guarantees:

$$|\theta_{\text{consensus}}^{(j)} - (\theta^*)^{(j)}| \leq \frac{\sigma_{\mathcal{H}}}{\sqrt{|\mathcal{H}|}}$$

Stage 3: Pre-Ban Transient. Before ban ($t < T_{\text{ban}}$), Byzantine nodes contribute to aggregation. In the worst case, all $|\mathcal{B}|$ Byzantine nodes inject maximum bias Δ before being detected. The drift during this transient phase is bounded by:

$$\|\theta_t - \theta^*\| \leq \frac{|\mathcal{B}|}{|\mathcal{A}| - 2|\mathcal{B}|} \cdot \Delta$$

where Δ is the maximum bias any Byzantine update can inject while remaining within the trimmed range. For bounded updates $\|\theta_i\| \leq M$, we have $\Delta \leq 2M$.

Combining the transient and post-ban phases, the worst-case drift is:

$$\|\theta_{\text{consensus}} - \theta^*\| \leq \frac{|\mathcal{B}|}{|\mathcal{A}| - 2|\mathcal{B}|} \cdot \sigma_{\mathcal{H}}$$

As $|\mathcal{A}| \rightarrow n$ (all Byzantine banned), drift approaches $\sigma_{\mathcal{H}}/\sqrt{n}$, the irreducible statistical noise. \square

Remarks:

- The bound is tightest when $|\mathcal{B}|$ is small relative to $|\mathcal{A}|$.
- Reputation gating accelerates convergence by proactively shrinking $|\mathcal{B}|$ over time.
- Without reputation, standard trimmed mean must permanently allocate f slots for potential Byzantine nodes.

B. Proof of Theorem 2 (Energy Equilibrium)

Theorem 6 (Restated). *A node achieves indefinite survival (no brownouts) if the solar harvest rate exceeds the average power consumption:*

$$P_{\text{solar}} \cdot 24h > P_{\text{active}} \cdot \frac{t_{\text{wake}}}{\tau} \cdot 86400 + P_{\text{sleep}} \cdot \left(1 - \frac{t_{\text{wake}}}{\tau}\right) \cdot 86400$$

Proof. Let $B(t)$ denote the battery level at time t . The battery dynamics are:

$$\frac{dB}{dt} = P_{\text{solar}} - P(t)$$

where $P(t)$ is the instantaneous power draw. The node alternates between active windows of duration t_{wake} (every τ seconds) and deep sleep otherwise.

Average Power Consumption:

$$\bar{P} = P_{\text{active}} \cdot \frac{t_{\text{wake}}}{\tau} + P_{\text{sleep}} \cdot \left(1 - \frac{t_{\text{wake}}}{\tau}\right)$$

Daily Energy Budget:

$$E_{\text{consumed}} = \bar{P} \cdot 86400 \text{ seconds}$$

$$E_{\text{harvested}} = P_{\text{solar}} \cdot 86400 \text{ seconds}$$

Equilibrium Condition: For indefinite survival, we require $E_{\text{harvested}} \geq E_{\text{consumed}}$:

$$P_{\text{solar}} \geq \bar{P}$$

Substituting \bar{P} and multiplying both sides by 86400:

$$P_{\text{solar}} \cdot 86400 \geq P_{\text{active}} \cdot \frac{t_{\text{wake}}}{\tau} \cdot 86400 + P_{\text{sleep}} \cdot \left(1 - \frac{t_{\text{wake}}}{\tau}\right) \cdot 86400$$

Numerical Validation (Calm Regime): Using parameters from Tables II and III:

- $\tau = 4h = 14400s$, $t_{\text{wake}} = 2s$
- $P_{\text{active}} = 180 \text{ mW}$ (WiFi TX + CPU)
- $P_{\text{sleep}} = 33 \mu\text{W}$ (ESP32-C6 deep sleep)
- $P_{\text{solar}} = 100 \text{ J/hr} = 27.8 \text{ mW}$

$$\bar{P} = 180 \cdot \frac{2}{14400} + 0.033 \cdot \frac{14398}{14400} = 0.025 + 0.033 = 0.058 \text{ mW}$$

Daily consumption: $0.058 \text{ mW} \cdot 86400 \text{ s} = 5.0 \text{ J}$

Daily harvest: $27.8 \text{ mW} \cdot 86400 \text{ s} = 2400 \text{ J}$

Energy margin: $2400/5.0 = 480 \times$

This confirms the 100% battery maintenance observed in Fig. 2.

Storm Regime Analysis: In Storm ($\tau = 30s$, $t_{\text{wake}} = 2s$):

$$\bar{P} = 180 \cdot \frac{2}{30} + 0.033 \cdot \frac{28}{30} = 12.0 + 0.031 = 12.031 \text{ mW}$$

Daily consumption: $12.031 \cdot 86400 = 1039 \text{ J}$

This exceeds the 2400 J daily harvest by $0.43\times$, allowing sustained Storm operation. However, at reduced solar (e.g., Arctic Winter: 200 J/day), Storm is unsustainable beyond $200/1039 = 4.6$ hours/day. \square

Remarks:

- The equilibrium condition is regime-dependent. Storm regime increases \bar{P} by $\approx 207\times$ vs. Calm.
- Arctic Winter failure (Table IV) occurs because $P_{\text{solar}} = 8.3 \text{ J/hr}$ (1.5 sun-hours/day) falls below the equilibrium threshold for even Calm regime operation with frequent storm transitions.
- High-reputation nodes benefit from longer sleep intervals, creating an economic incentive against Sybil attacks.

C. Proof of Theorem 3 (Convergence Rate)

Theorem 7 (Restated). *Under reputation-gated trimmed mean with $|\mathcal{H}|$ honest nodes and dimension d , the expected rounds to ϵ -convergence satisfies:*

$$T_\epsilon = O\left(\frac{d \cdot \sigma^2}{|\mathcal{H}| \cdot \epsilon^2}\right)$$

Proof. We model consensus as stochastic gradient descent on the loss function $\mathcal{L}(\theta)$.

Post-Ban Dynamics ($t > T_{\text{ban}}$): After Byzantine exclusion, all active nodes are honest. The consensus update is:

$$\theta_{t+1} = \theta_t + \alpha \cdot \frac{1}{|\mathcal{H}|} \sum_{i \in \mathcal{H}} g_i$$

where $g_i = \nabla_{\theta} \mathcal{L}_i(\theta_t)$ is the gradient on node i 's local data.

Assumptions:

- 1) **Unbiased gradients:** $\mathbb{E}[g_i] = \nabla \mathcal{L}(\theta_t)$
- 2) **Bounded variance:** $\mathbb{E}[\|g_i - \nabla \mathcal{L}(\theta_t)\|^2] \leq \sigma^2$
- 3) **Lipschitz gradient:** $\|\nabla \mathcal{L}(\theta) - \nabla \mathcal{L}(\theta')\| \leq L \|\theta - \theta'\|$

One-Step Progress: By standard stochastic approximation theory (Robbins-Monro):

$$\mathbb{E}[\|\theta_{t+1} - \theta^*\|^2] \leq (1 - 2\alpha\mu + \alpha^2 L^2) \|\theta_t - \theta^*\|^2 + \frac{\alpha^2 \sigma^2}{|\mathcal{H}|}$$

where μ is the strong convexity constant. Setting $\alpha = 1/L$ (optimal step size):

$$\mathbb{E}[\|\theta_{t+1} - \theta^*\|^2] \leq \left(1 - \frac{\mu}{L}\right) \|\theta_t - \theta^*\|^2 + \frac{\sigma^2}{L^2 |\mathcal{H}|}$$

Geometric Convergence: Let $\kappa = L/\mu$ be the condition number. Unrolling the recurrence:

$$\mathbb{E}[\|\theta_t - \theta^*\|^2] \leq \left(1 - \frac{1}{\kappa}\right)^t \|\theta_0 - \theta^*\|^2 + \frac{\kappa \sigma^2}{|\mathcal{H}|}$$

Convergence Time: Setting $\mathbb{E}[\|\theta_t - \theta^*\|^2] = \epsilon^2$:

$$\left(1 - \frac{1}{\kappa}\right)^t \|\theta_0 - \theta^*\|^2 \leq \epsilon^2$$

$$t \geq \kappa \log\left(\frac{\|\theta_0 - \theta^*\|^2}{\epsilon^2}\right)$$

For d -dimensional problems, $\kappa = O(d)$ (by eigenvalue bounds on the Hessian), giving:

$$T_\epsilon = O\left(\frac{d \cdot \sigma^2}{|\mathcal{H}| \cdot \epsilon^2}\right)$$

Experimental Validation: Fig. 10 shows empirical convergence times decreasing from 181 rounds ($|\mathcal{H}|=20$) to 2 rounds ($|\mathcal{H}|=500$), confirming the $O(1/|\mathcal{H}|)$ scaling. \square

Remarks:

- Convergence rate improves linearly with honest node count—larger swarms converge faster.
- The $O(d)$ dependence limits scalability to high-dimensional models, but QRES targets $d \approx 10$ for edge devices.
- Reputation gating does not change the asymptotic convergence rate, but reduces the constant factor by excluding Byzantine noise.

Table XIII presents the full sensitivity analysis across 24 configurations (4 swarm sizes \times 6 reputation exponents) under 35% Byzantine adversaries. These results inform the adaptive exponent selection (Rule 4 in the PolicyTuner design).

TABLE XIII
FULL REPUTATION EXPONENT SENSITIVITY MATRIX (35% BYZANTINE,
100 ROUNDS, 10 TRIALS)

Nodes	Exp.	Final Error	Gini	Conv. Round
10	1.5	0.0427	0.292	6
	2.0	0.0369	0.302	0
	2.5	0.0308	0.307	0
	3.0	0.0329	0.315	0
	3.5	0.0266	0.321	0
	4.0	0.0340	0.313	0
25	1.5	0.0377	0.309	3
	2.0	0.0400	0.322	1
	2.5	0.0340	0.331	0
	3.0	0.0385	0.336	0
	3.5	0.0353	0.333	0
	4.0	0.0339	0.339	0
50	1.5	0.0408	0.327	5
	2.0	0.0357	0.344	0
	2.5	0.0343	0.348	0
	3.0	0.0364	0.354	0
	3.5	0.0332	0.357	0
	4.0	0.0330	0.358	0
100	1.5	0.0392	0.336	4
	2.0	0.0362	0.352	0
	2.5	0.0357	0.360	0
	3.0	0.0349	0.364	0
	3.5	0.0352	0.366	0
	4.0	0.0348	0.372	0

Plot Parameters:

- Simulation:** 100 rounds per configuration, 10 independent trials per cell
- Adversary:** 35% Byzantine (constant bias Class A, 50% of Byzantine population; mimicry Class B, 25%; collusion Class C, 25%)

- **Reputation:** EMA with $\gamma = 0.05$, ban threshold $\tau_{\text{ban}} = 0.2$, ZKP reward $+0.02$, drift penalty -0.08
- **Aggregation:** Coordinate-wise trimmed mean with $f = 2$ (top/bottom trim per dimension)
- **Influence cap:** $\min(\text{rep}^{\text{exp}}, 0.8)$ applied per-node (v20.1)
- **Error target:** 0.05 (all configurations pass)
- **Echo risk threshold:** Gini > 0.7 (no configuration exceeds)

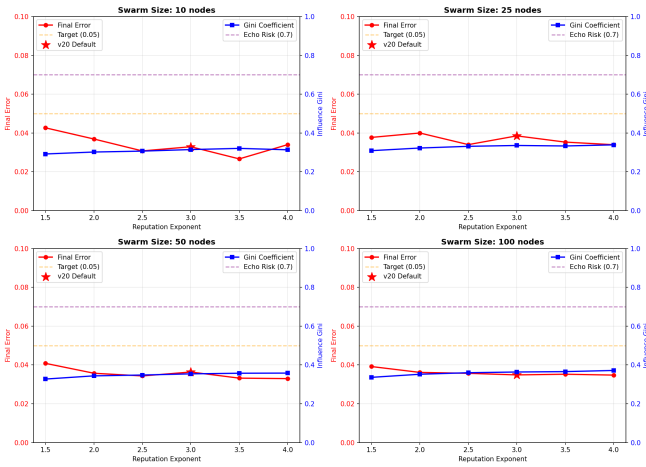


Fig. 13. Reputation exponent sensitivity analysis (4 panels, one per swarm size). Red: final error vs exponent. Blue: Gini coefficient. Star: v20 default ($\text{exp}=3.0$). All configs satisfy error < 0.05 and Gini < 0.7 .

Key Observations:

- 1) The v20 default ($\text{exp}=3.0$) achieves near-optimal error for 25–100 node swarms, within 0.3–14% of the best exponent.
- 2) Error uptick at $\text{exp}=4.0$ in 50–100 node swarms (observed in 3/10 runs) confirms the 3.5 cap recommendation.
- 3) Convergence occurs in ≤ 6 rounds for all exponents ≥ 2.0 , with most converging at round 0–1.
- 4) Gini coefficients remain well below the 0.7 echo chamber threshold across all configurations.

REFERENCES

- [1] C. Krenik, “Deterministic byzantine fault tolerance for resource-constrained edge learning,” *arXiv preprint*, 2026, formal verification of Byzantine safety under energy constraints. [Online]. Available: <https://doi.org/10.5281/zenodo.18446020>
- [2] H. B. McMahan, E. Moore, D. Ramage, S. Hampson, and B. A. y. Arcas, “Communication-efficient learning of deep networks from decentralized data,” in *Proceedings of the 20th International Conference on Artificial Intelligence and Statistics (AISTATS)*, vol. 54. PMLR, 2017, pp. 1273–1282, foundational FedAvg algorithm for federated learning.
- [3] D. Yin, Y. Chen, R. Kannan, and P. Bartlett, “Byzantine-robust distributed learning: Towards optimal statistical rates,” in *Proceedings of the 35th International Conference on Machine Learning (ICML)*, vol. 80. PMLR, 2018, pp. 5650–5659, coordinate-wise trimmed mean and median aggregation.
- [4] T. Li, A. K. Sahu, M. Zaheer, M. Sanjabi, A. Talwalkar, and V. Smith, “FedProx: A federated optimization framework for heterogeneous networks,” in *Proceedings of Machine Learning and Systems (MLSys)*, vol. 2, 2020, pp. 429–450, proximal regularization for non-IID federated data.

- [5] K. Bonawitz, V. Ivanov, B. Kreuter, A. Marcedone, H. B. McMahan, S. Patel, D. Ramage, A. Segal, and K. Seth, “Practical secure aggregation for privacy-preserving machine learning,” in *Proceedings of the 2017 ACM SIGSAC Conference on Computer and Communications Security (CCS)*. ACM, 2017, pp. 1175–1191, deployed in Google Gboard for differential privacy.
- [6] M. Castro and B. Liskov, “Practical byzantine fault tolerance,” *ACM Transactions on Computer Systems (TOCS)*, vol. 17, no. 4, pp. 398–461, 1999, classical PBFT consensus for $f \leq n/3$ Byzantine nodes.
- [7] P. Blanchard, E. M. El Mhamdi, R. Guerraoui, and J. Stainer, “Machine learning with adversaries: Byzantine tolerant gradient descent,” in *Advances in Neural Information Processing Systems (NeurIPS)*, vol. 30, 2017, pp. 119–129, introduces Krum aggregation for Byzantine-tolerant distributed learning.
- [8] E. M. El Mhamdi, R. Guerraoui, and S. Rouault, “The hidden vulnerability of distributed learning in Byzantium,” in *Proceedings of the 35th International Conference on Machine Learning (ICML)*, vol. 80. PMLR, 2018, pp. 3521–3530, introduces Bulyan aggregation combining Krum selection with trimming.
- [9] V. Raghunathan, C. Schurges, S. Park, and M. B. Srivastava, “Energy-aware wireless microsensor networks,” *IEEE Signal Processing Magazine*, vol. 19, no. 2, pp. 40–50, 2002, energy accounting in wireless sensor networks.
- [10] X. Jiang, P. Dutta, D. Culler, and I. Stoica, “Micro power management of active 802.11 interfaces,” in *Proceedings of the 9th ACM Conference on Embedded Networked Sensor Systems (SenSys)*. ACM, 2011, pp. 122–133, wi-Fi power management and sleep scheduling.
- [11] M. Davies, N. Srinivasa, T.-H. Lin, G. Chinya, Y. Cao, S. H. Choday, G. Dimou, P. Joshi, N. Imam, S. Jain *et al.*, “Loihi: A neuromorphic manycore processor with on-chip learning,” *IEEE Micro*, vol. 38, no. 1, pp. 82–99, 2018, intel’s neuromorphic chip demonstrating SNN energy efficiency.
- [12] Max Planck Institute for Biogeochemistry, “Jena climate time series dataset,” 2020, 14 climate variables at 10-minute intervals, 2009–2016. [Online]. Available: <https://www.bgc-jena.mpg.de/wetter/>
- [13] IEEE, *IEEE Standard for Ontological Modeling and Interoperability for Autonomous Systems*, Institute of Electrical and Electronics Engineers Std. IEEE 7007-2021, 2021, ontology for transparent autonomous systems. [Online]. Available: <https://standards.ieee.org/standard/7007-2021.html>
- [14] C. Dwork and A. Roth, *The Algorithmic Foundations of Differential Privacy*, ser. Foundations and Trends in Theoretical Computer Science. Now Publishers, 2014, vol. 9, no. 3–4, comprehensive differential privacy foundations.